RESEARCH PAPER

Cation Distribution of Co-Ni-Mn Ferrites from Magnetization and Magnetostriction

Pradnya K. Chougule[2], Pranali P. Chavan[2], Amit R. Yaul[3], Gourav B. Pethe[3], Avinash A. Ramteke[1],*

* dravinash03@gmail.com

[1] Départment of Chemistry, Devchand Collège, Arjunnagar, Dist.: Kolhâpur, Maharashtra, INDIA

[2] Départment of Physics, Devchand Collège, Arjunnagar, Dist.: Kolhâpur, Maharashtra, INDIA

[3] Départment of Chemistry, Narayanrao Kale Smruti Model College, Karanja (Gh.), Dist.: Wardha, Maharashtra, INDIA

Abstract: Nickel-doped CoMn ferrites with high magnetization were synthesized by double sintering solid state route with compositions of $Co_{0.7-x}Ni_xMn_{0.3}Fe_2O_4$ with x= 0, 0.05, 0.1 and 0.15. Theoretical Cation distribution for cubic spinel ferrites was suggested based on electrical configuration expectations and cation site preferences. The cation distribution suggested was in good agreement with experimental results obtained from VSM and XRD. Values of theoretically calculated magnetic moment, coercivity and magnetization are in good agreement with experimental data obtained from VSM. Maximum saturation magnetization of 37.7emu/gm is obtained for sample $Co_{0.7}Mn_{0.3}Fe_2O_4$ at a magnetic field of 5 K Oe. Magnetostriction was found to increase with increasing magnetic field (from 1 KOe to 5 KOe.) Maximum magnetostriction of 84 ppm was observed for sample $Co_{0.7}Mn_{0.3}Fe_2O_4$ at 5 KOe. Maximum magnetization of magnetoelectric composites with 30% $Co_{0.7-x}Ni_xMn_{0.3}Fe_2O_4$ – 70% $PbZr_{0.48}Ti_{0.52}$ was found to be 7.4 emu/g for composition with x= 0.

Keywords: Co-Ni-Mn Ferrites, Cation Distribution, Magnetostriction, Nickel doped, M-H Hysteresis loop.

1. INTRODUCTION

Ferrites have been of great interest due to their potential applications in sensors, hyperthermia, catalysts and targeted drug delivery [1]. Ferrites are ferromagnetic materials with the general formula MFe_2O_4 where M is a divalent metallic ion like Co^{2+}, Ni^{2+}, Mn^{2+} etc [2]. The unit cell of the cubic spinel structure of ferrites consists of eight formula units with 32 oxygen atoms occupying the FCC lattice. Metallic ions can occupy vacancies formed by oxygen ions [3]. Two types of occupancy sites are formed as 64 - tetrahedral site (A site), surrounded by four oxygen ions and 32 - octahedral site (B - site) surrounded by six oxygen ions. Among 64 available A sites only 8 are occupied by metallic cations while other cations reside at 16 octahedral sites. Cation distribution for normal, inverse and mixed spinel structure is given by,

Normal spinel structure - $[8M^{2+}]_{tet} [16Fe^{3+}]_{oct}$
Inverse spinel structure - $[8Fe^{3+}]_{tet} [8M^{2+} 8Fe^{3+}]_{oct}$
Mixed spinel structure - $[(1-x) M^{2+} 8Fe^{3+}]_{tet} [xM^{2+} 8Fe^{3+}]_{oct}$

[4]. According to two sublattice models, the magnetic behavior of ferrites strongly depends on the A-B exchange interaction [5]. The distribution of cations among A site and B site will decide the properties of ferrites [6]. Thus, cation distribution obtained from theoretically and experimentally calculated data was compared for all compositions of $Co_{0.7-x}Ni_xMn_{0.3}Fe_2O_4$. Cobalt ferrite is well known for high magnetization, high coercivity, lower resistivity, high magnetic stability and good mechanical hardness [7]. The incorporation of Mn enhances magnetization and magnetostriction of cobalt ferrite [8]. Nickel ferrite has the highest resistivity among all spinel ferrite [9]. Doping of nickel may enhance the resistivity of Co-Mn ferrites [10], making $Co_{0.7-x}Ni_xMn_{0.3}Fe_2O_4$ with x= 0, 0.05, 0.1 and 0.15 suitable candidate as a magnetic phase of Magnetoelectric composites. A magnetoelectric composite with higher resistivity of the magnetostrictive ferrite phase is expected to give a high magnetoelectric coefficient [11]. Thus 30% $Co_{0.7-x}Ni_xMn_{0.3}Fe_2O_4$ –70% $PbZr_{0.48}Ti_{0.52}$ is expected suitable candidate to obtain higher magnetoelectric potential for sensor applications [12].

2. EXPERIMENTAL PROCEDURES

All the compositions of $Co_{0.7-x}Ni_xMn_{0.3}Fe_2O_4$

(with x= 0.00, 0.05, 0.10 and 0.15) were synthesised [13] by the solid-state reaction route. The stoichiometric ratio of starting materials NiO, CoO, Fe_2O_3, and Mn_2O_3 was presintered at 900°C for 10 hours and final sintering was carried out at 1100°C for 11 hours. Powder method XRD spectrometer Model: PW 3710/ PW1710 PHILIPS, Holland and Bruker D8 was used for phase confirmation. The surface morphology of samples was recorded by scanning electron microscope JEOL, Model JSM – 6360A. LAKESHORE 7307 model vibrating sample magnetometer was used to trace M-H hysteresis loops.

3. RESULTS AND DISCUSSION

3.1. X-ray Diffraction Patterns

At room temperature X-ray diffraction patterns of $Co_{0.7-x}Ni_xMn_{0.3}Fe_2O_4$ (with x= 0.00, 0.05, 0.10 and 0.15) compositions and 30%CNMF-70%PZT magnetoelectric composites are obtained.

The room temperature powder X-ray diffraction patterns of $Co_{0.7-x}Ni_xMn_{0.3}Fe_2O_4$ compositions (with x= 0.00, 0.05, 0.10, and 0.15) are presented in Fig. 1. The diffraction patterns indicate a cubic spinel ferrite phase characterized by excellent crystallinity, and all peaks are successfully indexed using JCPDS card Nos. 77-0426. All spinel exhibits a cubic structure with equal lattice parameters (a= b= c) and right angles (α= β= γ= 90°), falling under space group Fd3m (227). The lattice parameters consistently range from 8.0 Å to 8.6 Å.
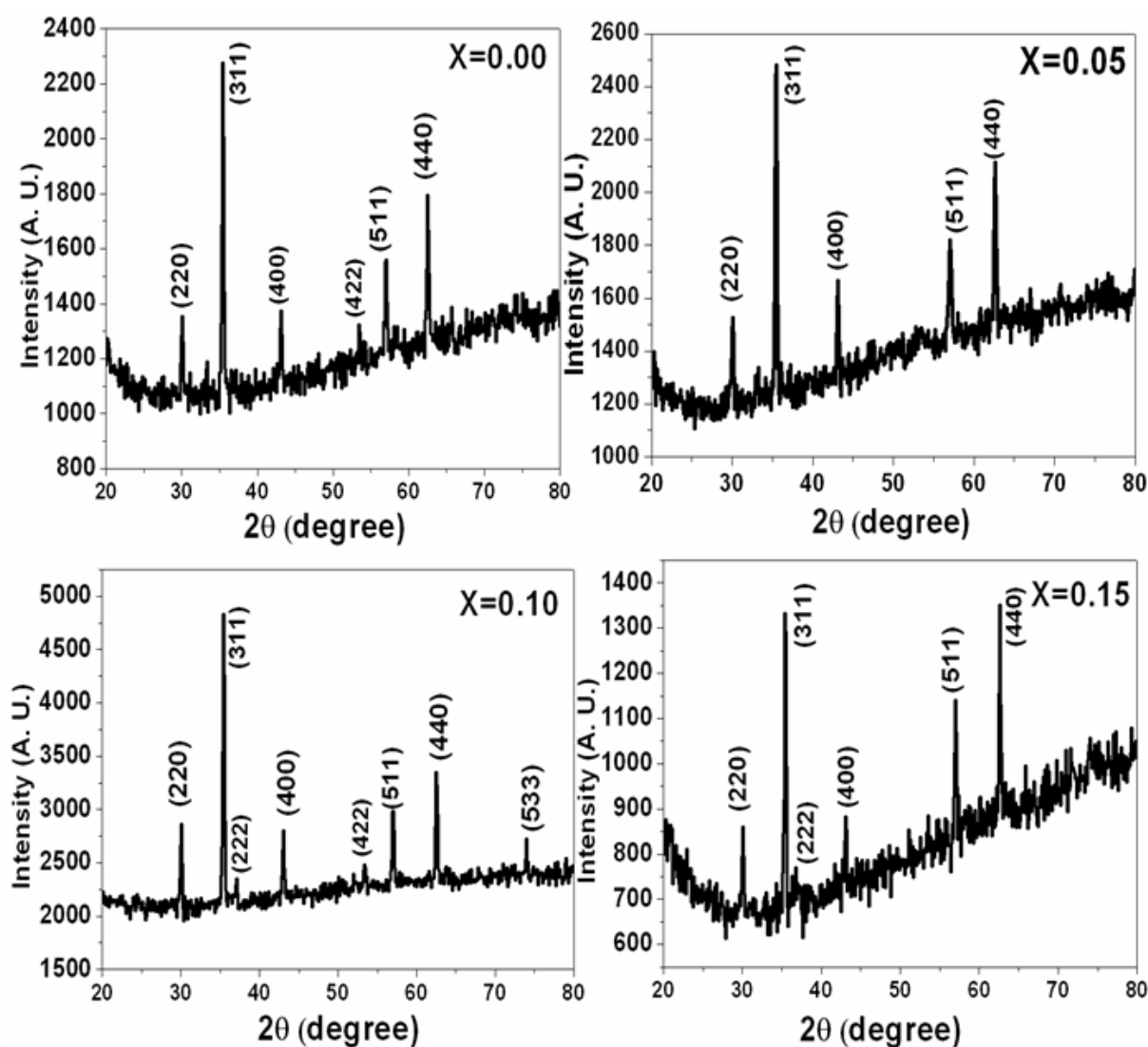

Fig. 1. X-ray diffraction patterns of $Co_{0.7-x}Ni_xMn_{0.3}Fe_2O_4$ ferrite (x= 0.00, 0.05, 0.10 and 0.15)

The lattice parameter was determined using the formula $a = d\sqrt{(h^2 + k^2 + l^2)}$, where a is the lattice parameter, d is the interplanar distance, and (h k l) represents Miller indices. The cell volume, dependent on ionic radius and cation distribution, generally follows a linear trend in solid solutions of spinels. In this case, the lattice parameter decreases linearly with an increase in Ni content, adhering to Vegard's law. This is attributed to the substitution of Co^{2+} ions (ionic radius of 0.78 Å) by Ni^{2+} ions (ionic radius of 0.74 Å), resulting in a decrease in lattice parameter from 8.41 Å to 8.37 Å. The obtained results align well with reported values, confirming the structural changes induced by varying Ni concentrations.

3.2. Scanning Electron Micrographs

SEM micrographs of the $Co_{0.7-x}Ni_xMn_{0.3}Fe_2O_4$ (with x= 0.00, 0.05, 0.10 and 0.15) sintered at 1100°C for 11 hours, and 30%CNM ferrites-70%PZT magnetoelectric composites sintered at 900°C has been published [14]. SEM micrographs in Fig. 2 (a-d), depict the morphological characteristics of $Co_{0.7-x}Ni_xMn_{0.3}Fe_2O_4$ samples sintered at 1100°C for 11 hours, with varying Ni content (x= 0.00, 0.05, 0.10, and 0.15). Notably, all samples exhibit small pores with well-established contacts among grains, and as Ni content increases, the samples show increased density. The average grain size, determined using the line intercept method, reveals a significant decrease from 1 μm for x= 0.00 (CMF) in Fig. 2(a) to 0.4 μm for x= 0.15 (CNMF) in Fig. 2 (d). This reduction in grain size correlates with the substitution of Ni^{2+} (ionic radius 0.74 Å), which is smaller than Co^{2+} (ionic radius 0.78 Å). The SEM results align with X-ray diffraction findings, indicating lattice contraction with rising Ni content. Additionally, an increase in the number of grain boundaries and porosity is observed with higher Ni content, particularly in the x= 0.15 composition, suggesting an expected higher DC resistivity. Table 1, summarizes the grain size and lattice parameter values for all compositions, showcasing the trend of decreasing grain size and lattice constant with increasing Ni content.
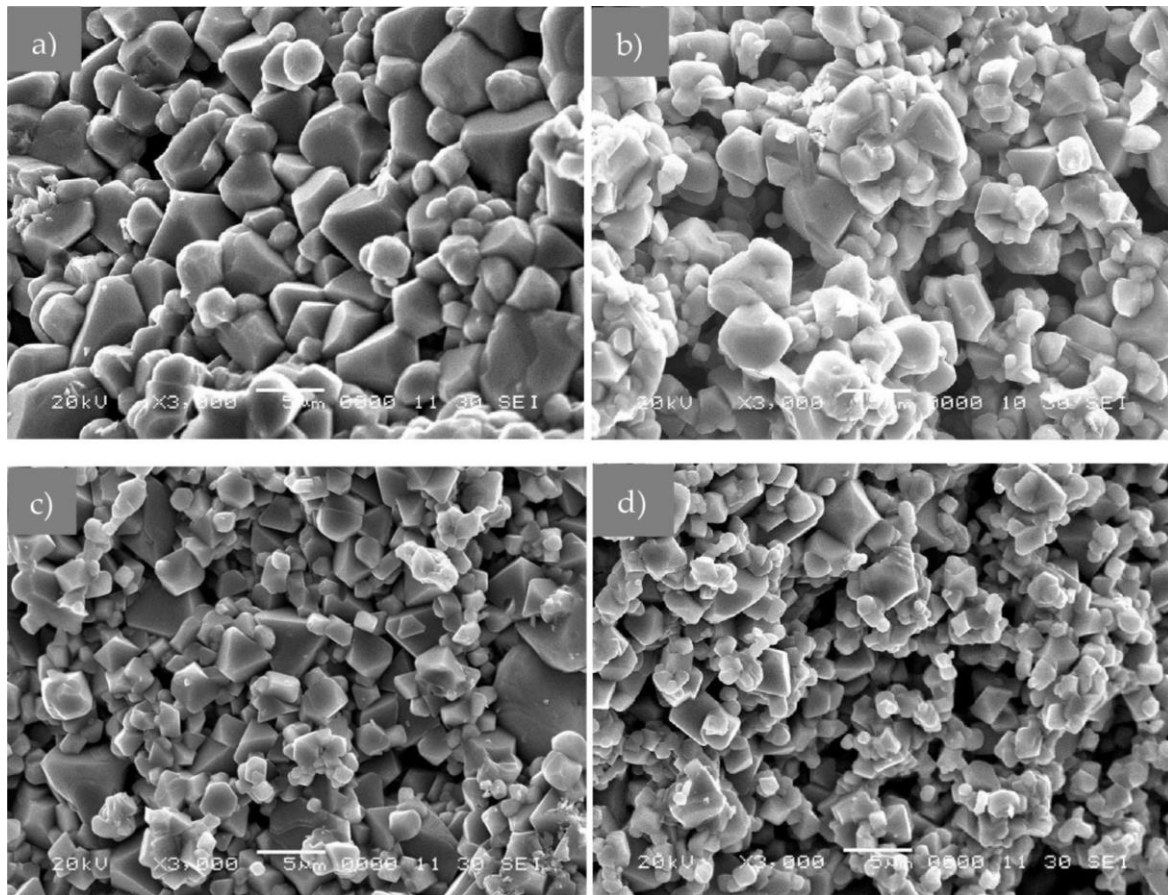

Fig. 2. (a) SEM micrographs of $Co_{07}Mn_{0.3}Fe_2O_4$ (b) SEM micrographs of $Co_{0.65}Ni_{0.05}Mn_{0.3}Fe_2O_4$ (c) SEM micrographs of $Co_{0.6}Ni_{0.1}Mn_{0.3}Fe_2O_4$ (d) SEM micrographs of $Co_{0.55}Ni_{0.15}Mn_{0.3}Fe_2O_4$

3.3. M-H Hysteresis Loop
a) ferrites

The plots (Fig. 3) of magnetization (M) vs applied field (H) help in understanding the magnetic response of the material and provide information about the magnetic parameters (reported in Tables 1 and 2) such as saturation magnetization (M.), coercivity (H.) and remanence magnetization (M.). The Fig. 3 and Fig. 4 (Fig. 4 reported by Chougule P.K. *et.al* [15] shows the M-H curves for different compositions of $ConNiMnasFe_2O_4$ ferrite pellets with x= 0.00, 0.05, 0.10 and 0.15.
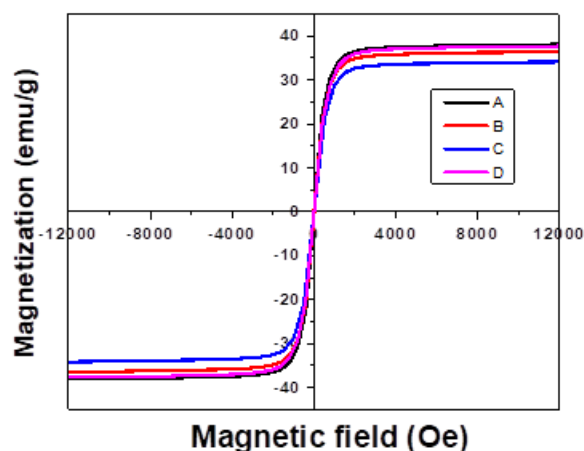
octahedral sites. The magnetic moment for Co^{2+} ions (3 µB) is more than that for Ni^{2+} ions (2B). Therefore, the decreasing Co^{2+} concentration on the octahedral sites may result in a decreasing magnetic moment per formula of $Co_{0.7}$-$Ni_xMn_{0.3}Fe_2O_4$. The possibility of mixed valencies of Mn (Mn^{2+} and Mn^{3+}) cannot be denied in the preparation of Co-Ni_x $Mn_{0.3}$ Fe_2O_4 ferrites. The substitution of Fe^{3+} by Mn3 is expected to decrease the magnetization assuming that the substituted Mn^{3+} ions preferentially occupy the octahedral B-site.

Fig. 3. VSM of $Co_{0.55}Ni_{0.15}Mn_{0.3}Fe_2O_4$.

In Fig. 3 and Fig. 4, these plots show that an increase in Ni^{2+} content reduces the magnetization of cobalt ferrite, which may be due to the substitution of Ni^{2+} ions by Co^{2+} ions on the
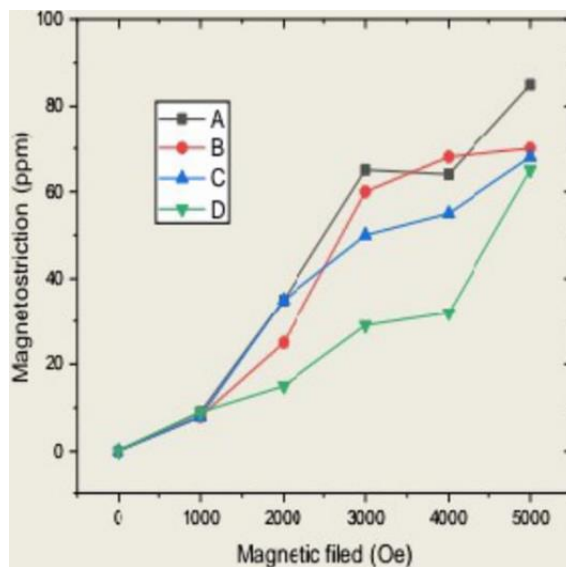

Fig. 4. Variation of magnetostriction with magnetic field for $Co_{0.7-x}Ni_xMn_{0.3}Fe_2O_4$ pallets with x= 0.00, 0.05, 0.10 and 0.15.

Table 1. Values of grain size and lattice parameter with Ni content

Ni content	Grain size (µm)	Lattice constant (Å)
0.00	1	8.41
0.05	0.9	8.41
0.10	0.7	8.40
0.15	0.4	8.40

Table 2. Values of bond lengths, site radii, calculated and observed values of magnetic moments and Y-K angles with Ni content

X	Cation distribution	Bond lengths (Å)		Radius of sites (Å)		Calculated magnetic moment (µB)	Experimental magnetic moment (µB)	Y-K angles
		R_A	R_B	r_A	r_B			
0.00	$(Fe^{3+} Mn_{0.3}^{2+})_A [C0_{0.7}^{2+} Fe^{3+}]_B$	1.734	2.054	0.471	0.753	1.6	1.11	47 93′
0.05	$(Fe^{3+}Mn_{0.3}^{2+})_A[C0_{0.65}^{2+}Ni_{0.05}^{2+}Fe^{3+}]_B$	1.734	2.054	0.471	0.753	2.55	2.22	$39^0 64$
0.1	$(Fe^{3+} Mn_{0.3}^{2+})_A[C0_{0.6}^{2+}Ni_{0.1}^{2+}Fe^{3+}]_B$	1.732	2.052	0.469	0.751	1.5	1.93	$44^0 73′$
0.15	$(Fe^{3+}Mn_{0.3}^{2+})_A[C0_{0.55}^{2+}Ni_{0.15}^{2+}Fe^{3+}]_B$	1.731	2.051	0.469	0.750	1.45	1.19	$53^0 13′$

4

This is due to the decrease in the magnetic moment from 5 µB for Fe to 4 µB for Mn3. On the other hand, the substitution of Co^{2+} by Mn^{2+} should enhance the magnetization since the magnetic moments for Co^{2+} and Mn^{2+} are 3 up and 5 µB, respectively. Further, it is reported that at lower concentrations, Mn^{2+} ions are substituted in the B site having a magnetic moment of 5 µB which is equivalent to the magnetic moment of Fe^{3+} ion. Therefore, it may be concluded that if the formation of Mn^{2+} ions took place at a lower concentration of Mn, it does not effect on magnetization of ferrite systems. Shows M-H curves for different compositions of $Co_{0.7-x}Ni_xMn_{0.3}Fe_2O_4$ with x= 0.00, 0.05, 0.10 and 0.15.

M-H hysteresis loops show a decrease in magnetization with an increase in Ni content. This decrease in magnetization is attributed to the replacement of Co^{2+} ions by Ni^{2+} ions at the B - site. The magnetic moment of Co^{2+} ions (3 µB) is more than Ni^{2+} ions (2 µB). Therefore, a decrease in the concentration of Co^{2+} ions on the B site results in a decrease in magnetization per formula unit. The magnetic moment per formula unit is calculated by using the formula,

$$\mu B = \frac{M \times Ms}{5585}$$

and coercivity was calculated by using the formula,

$$Hc = \frac{0.96 \times K}{Ms}$$

In spinel ferrites, the relative size and charge of the cations, compared to the lattice site is an important consideration for cation distribution in ferrites, against ideal tetrahedral and octahedral site radii of 0.54 A^0 and 0.64 A^0 respectively. The divalent ions are generally larger than the trivalent ions as; the larger nuclear charge of trivalent ion produces greater electrostatic attraction and so pulls the outer orbits inwards. Generally, the trivalent ions occupy smaller tetrahedral (A) sites and the divalent ions occupy larger octahedral (B) sites. Electrical configuration expectation for Co^{2+} and Ni^{2+} also has strong preferences for B-site. The exception is found in pure $MnFe_2O_4$ which is a mixed spinel structure, where nearly 20% of Mn is distributed as Mn^{2+} in the B- site and the remaining 80% of Mn^{2+} is distributed in the A-site. Thus, cation distribution suggested for $Co_{0.7}Mn_{0.3}Fe_2O_4$, can be given by,

$(Fe^{3+}Mn^{2+}_{0.3})_A [Co^{2+}_{0.7}Fe^{3+}]_B$
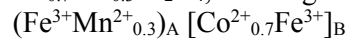
As Ni has a strong preference for B-site, general cation distribution for ferrite under consideration can be given as,

$(Fe^{3+}Mn^{2+}_{0.3})_A[Co^{2+}_{0.7-x}Ni^{2+}_xFe^{3+}]_B$
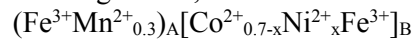
represents experimental data of saturation magnetization, coercivity, magnetic moment per formula unit and anisotropy constant obtained from VSM. Table 3 and Table 4 show that, values of saturation magnetization, coercivity, magnetic moment and anisotropy constant decrease with an increase in Ni content.

b) Magnetoelectric composites

Table 4, shows the variation of magnetization with increasing magnetic field for [30%] CoNi, $MnasFe_2O_4+$ [70%] PZT with x= 0.00, 0.05, 0.10 and 0.15. For all the compositions of ME composites, magnetization increases rapidly at lower magnetic fields and at higher magnetic fields it attains a constant saturation value. Variation of saturation magnetization is not linear with Ni content.

Table 3. Variation of saturation magnetization, coercivity, magnetic moment and anisotropy constant for $Co_{0.7}Ni_xMn_{0.3}Fe_2O_4$ pellets with x= 0.00, 0.05, 0.10 and 0.15.

Ni content x	Ms(emu/gm)	Hc(emu/gm)	µB	K
0	37.7	50.3	1.11	1975.32
0.05	37.6	46.6	2.22	1825.16
0.10	36.42	40.7	1.93	1544.05
0.15	34.02	39.2	1.19	1389.1

Table 4. Variation of saturation magnetization, Bhor magneton, coercive field and anisotropy constant with Ni content for ME composite pellets of [30%] $Co_{0.7}Ni_xMn_{0.3}Fe_2O_4+$ [70%] PZT with x= 0.00, 0.05, 0.10 and 0.15.

Ni content x	Ms(emu/gm)	Hc(emu/gm)	µB	K
0	7.4	300.3	0.39	2314.8
0.05	6.69	175.4	0.35	1222.3
0.10	6.47	170.3	0.34	1147.7
0.15	6.32	145.2	0.33	955.9

The maximum value of saturation magnetization is observed for the composition with Ni content of 0.05 and it can be expected to obtain higher ME output voltage and higher ME coefficient with this particular composition. It is accepted that the magnetic properties of ME composites are entirely due to ferrites since ferroelectric materials are completely non-magnetic. In the case of ferrites, magnetization was found to decrease linearly with Ni content but in the case of ME composites, this linear variation is not observed. This is because ferrite and ferroelectric grains are randomly mixed. Thus, compositions in which ferrite grains are dispersed closer to each other may show higher magnetization and compositions in which ferrite grains are dispersed at greater distances may show lower magnetization due to breaking of magnetic loops. Shows a variation of saturation magnetization, Bhor magnetron and anisotropy constant for ME composites with Ni content. Variation of all above-mentioned properties is also not linear with Ni content.

3.4. Magnetostriction of Ferrites

It is now well known that, a change in the dimension of magnetic material caused by a change in its magnetic state is expressed in terms of magnetostriction, Frequently, magnetostriction is experimentally observed in terms of change in dimension by the change in magnitude or direction of applied magnetic field. The following are important types of magnetostriction: (a) Longitudinal Joule magnetostriction which is a change in linear dimension parallel to an applied magnetic field, (b) Transverse magnetostriction which is a change in dimensions perpendicular to an applied magnetic field and (c) Volume magnetostriction. In the most common type of magnetostriction i.e. Joule magnetostriction, the dimensional change is associated with the distribution of distorted magnetic domains. In a demagnetized state, the domains are distributed such that the net external magnetization of the body is zero. In a material exhibiting Joule magnetostriction, each domain is distorted by inter-atomic force in such a way as to minimize the total energy.

In a body with negative magnetostriction, the dimension along the direction of magnetization is shortened, while the one perpendicular to it is elongated. Fig. 3 shows the variation of magnetostriction with magnetic field for Co Ni, MnO $3Fe_2O_4$ ferrite pellets with x= 0.00, 0.05, 0.10 and 0.15. Magnetostriction increases with an increase in magnetic field for all the compositions of ferrites. Careful observation shows that magnetostriction decreases with an increase in Ni content. It is reported that magnetostriction decreases with a decrease in grain size. From X-ray diffraction and SEM studies, it was observed that grain size decreases with an increase in Ni content. Observed values of magnetostriction are in good agreement with reported values. Pure cobalt ferrite shows higher magnetostriction an all-spinel ferrite. It is also reported that the addition of a small amount of Mn will enhance the magnetostriction of pure cobalt ferrite but the addition of Ni content may decrease magnetostriction due to the dilution effect.

4. CONCLUSIONS

The cation distribution of mixed ferrites can be evaluated theoretically by XRD analysis and experimentally by magnetization measurement. Theoretical and experimental calculations of magnetic moments are in good agreement with each other. From these results, it can be suggested that Co^{2+} and Ni^{2+} ion prefers the B site whereas Mn^{2+} ions prefer the A site. Thus cation distribution of $Co_{0.7-x}Ni_xMn_{0.3}Fe_2O_4$ mixed ferrite is given by $(Fe^{3+} Mn0.32+)A[C01-x2+Nix2+Fe3+]B$. Maximum saturation magnetization of 37.7 emu/gm is obtained for sample $Co_{0.7}Mn_{0.3}Fe_2O_4$ at a magnetic field of 5 K Oe. Due to the addition of nickel with a lower magnetic moment of 2 μB, as compared to cobalt (3 MB0 magnetization decreases with the addition of nickel content. Magnetostriction was also found to decrease with an increase in N with an increasing magnetic field.

CONFLICTS OF INTEREST

There are no conflicts to declare including any competing financial interest.

ACKNOWLEDGEMENTS

of characterization techniques

REFERENCES

[1]. Raturi, P., Khan, Iliyas, Joshi, Gaurav, Kumar, Samir and Gupta, Sachin, "Ferrite Nanoparticles for Sensing Applications", Engineered Ferrites and Their Applications Materials Horizons: From Nature to Nanomaterials, doi.org/10.1007/978-981-99-2583-4_9 2023, p. 151–187.

[2]. Dippong, T., Levei, E.A., and Cadar, O., "Effect of Transition Metal Doping on the Structural, Morphological, and Magnetic Properties of $NiFe_2O_4$", Materials (Basel), 2022, 15(9), 2996.

[3]. Satalkar, M., and Kane, S. N., "On the study of Structural properties and Cation distribution of $Zn_{0.75-x}Ni_xMg_{0.15}Cu_{0.1}Fe_2O_4$ nano ferrite: Effect of Ni addition", Phys. Conf. Ser., 2016, 755, 012050.

[4]. Heiba, Z.K., Mostafa, N.Y., and Abd Elkader, O.H., November "Structural and magnetic properties correlated with cation distribution of Mo-substituted cobalt ferrite nanoparticles", Materials Science, Chemistry; Journal of Magnetism and Magnetic Materials, 2014, 368, 246-251.

[5]. Lakshmi, M., Vijaya Kumar, K., and Thyagarajan, K., "An investigation of structural and magnetic properties of Cr–Zn ferrite nanoparticles prepared by a sol–gel process", Journal of Nanostructure in Chemistry, 2015, 5(4), 365-373.

[6]. Bamzai, K.K., Kour, Gurbinder, Kaur, B., Kulkarni, S.D., "Effect of cation distribution on structural and magnetic properties of Dy substituted magnesium ferrite", Journal of Magnetism and Magnetic Materials, 2013, 327, 159-166.

[7]. Cedeño-Mattei, Y., Perales-Pérez, O., Uwakweh, O.N.C., "Synthesis of high-coercivity non-stoichiometric cobalt ferrite nanocrystals: Structural and magnetic characterization", Materials Chemistry and Physics, 2012, Volume 132, Issues 2–3, 999-1006.

[8]. Bhame, S.D., and Joy, P.A., "Magnetic and magnetostrictive properties of manganese substituted cobalt ferrite", Journal of Physics D: Applied Physics, 2007, 40 (11), 3263.

[9]. Narang, S.B., and Pubby, K., Nickel Spinel Ferrites: A review, Journal of Magnetism and Magnetic Materials, 2021, 519, 167163.

[10]. Debnath, S., and Das, R., "Cobalt doping on nickel ferrite nanocrystals enhances the micro-structural and magnetic properties: Shows a correlation between them", Journal of Alloys and Compounds, 2021, 852, 156884.

[11]. Begum, S.S., Bhavana, H.V., and Bellad, S.S., "Dielectric and magnetoelectric behavior of $Ni_xCu_{1-x}Fe_2O_4$–$PbZr_{0.52}Ti_{0.48}O_3$ laminated multilayered nanocomposites", Indian Journals of Physics, 2023, 97, 115–120.

[12]. Sun, K., Jiang Z., Wang C., Han D., Yao Z., Zong W., Jin Z., and Li S., "High-Resolution Magnetoelectric Sensor and Low-Frequency Measurement Using Frequency Up-Conversion Technique", Sensors, 2023, 23(3), 1702.

[13]. Agusu, L., Crystal and microstructure of $MnFe_2O_4$ synthesized by ceramic method using manganese ore and iron sand as raw materials, Journal of Physics: Conference Series, 2019, 1153(1), 012056.

[14]. Chougule, P.K., Kumbhar, S.S., Kolekar, Y.D., Bhosale, C.H., Enhancement in Curie temperature of nickel substituted Co–Mn ferrite, Journal of Magnetism and Magnetic Materials, 2014, 372, 181-186.

[15]. Chougule, P.K., Kolekar, Y.D., Kolekar and C. H. Bhosale, C.H., Linear and quadratic magnetoelectric effect in CNMFO: PZT magnetoelectric composite, Journal of Materials Science: Materials in Electronics, 2013, 24 (10), 3856-3861.